JACS
JOURNAL OF THE AMERICAN CHEMICAL SOCIETY

Communication

pubs.acs.org/JACS

Time-Resolved Structural Evolution of Additive-Processed Bulk Heterojunction Solar Cells

James T. Rogers,[‡] Kristin Schmidt,[‡,§] Michael F. Toney,[§] Guillermo C. Bazan,*[,†] and Edward J. Kramer*[,‡,∥]

[†]Center for Polymers and Organic Solids, Department of Chemistry & Biochemistry, University of California, Santa Barbara, California 93106, United States

[‡]Department of Materials, University of California, Santa Barbara, California 93106, United States

[§]Stanford Synchrotron Radiation Lightsource, SLAC National Accelerator Laboratory, Menlo Park, California 94025, United States

[∥]Department of Chemical Engineering, University of California, Santa Barbara, California 93106, United States

Supporting Information

ABSTRACT: Solution deposition using high-boiling-point additives such as octanedithiol (ODT) provides a simple and widely used fabrication option for improving the power conversion efficiencies of solar cells composed of narrow-band-gap conjugated polymer donor/fullerene acceptor blends. Previous examination of the resulting device active layers has shown that the use of additives influences the degree of phase segregation within the bulk heterojunction (BHJ) blend and also improves ordering within the polymeric domains. In this work, in situ grazing-incidence wide-angle X-ray scattering as a function of time was used to explore the dynamics of the BHJ evolution. These studies showed that a small percentage of ODT in chlorobenzene (CB) induced the nucleation of polymeric crystallites within 2 min of deposition, increased the orientational order of specific polymorphs, and promoted further crystallite nucleation over a period longer than 40 min after casting. Similar structural changes did not occur when the same BHJ blend was cast from pure CB.

Conjugated polymer solar cells processed from solution are currently the object of intense study.[1,2] Molecular design parameters exist for donor polymers to achieve appropriate absorption of the solar spectrum while simultaneously controlling molecular orbital energy levels to enable charge transfer to acceptor components, especially fullerenes, in order to maintain high device open-circuit voltages.[3] The most successful devices use a blend comprising donor and acceptor components that form a bulk heterojunction (BHJ) morphology in which discrete phases of the two components form a nanoscale phase-separated bicontinuous network.[4] The optoelectronic properties of BHJ blends are therefore a convolution of the molecular features of the individual components as well as the three-dimensional (3D) organization of these components in the bulk.[5] Developing control over the molecular properties and bulk nanoscale organization is therefore necessary for reliable fabrication of BHJ devices with high power conversion efficiencies (PCEs).

Despite the vast array of conjugated polymer architectures that have been synthesized, there exist very few solution processing techniques capable of modifying the BHJ organization, particularly at the time of film deposition. One of the most widely utilized approaches involves adding small quantities of high-boiling-point additives to the solution from which the BHJ blend is cast.[6−8] This approach was originally demonstrated for a blend of poly{2,1,3-benzothiadiazole-4,7-diyl[4,4-bis(2-ethylhexyl)-4*H*-cyclopenta[2,1-*b*:3,4-*b*′]-dithiophene-2,6-diyl]} (PCPDTBT, Scheme 1) and [6,6]-phenyl C_{71} butyric acid methyl ester ($PC_{70}BM$, Scheme 1), where the addition of 2−3% octanedithiol (ODT) to the chlorobenzene (CB) solution was shown to increase the PCE significantly, from 3.3 to 5.5%.[9] Efforts to characterize the origin of this improvement revealed that additives affect the degree of phase separation between the blend components as well as the polymorph, size, perfection, and population of PCPDTBT crystallites.[9−13] Since this discovery, new additives have been identified, and the technique has been shown to be applicable to a wide range of BHJ blend compositions; the use of additive processing can be observed repeatedly in reports detailing the fabrication procedures of record-efficiency cells.[14−16] Understanding why additive processing finds such general applicability is an important requirement for future materials design and provides a path toward rational optimization of device performance.

In spite of microstructural characterization data demonstrating how additives influence the final BHJ blend structure, little

Scheme 1. Molecular Structures of (a) PCPDTBT and (b) $PC_{70}BM$

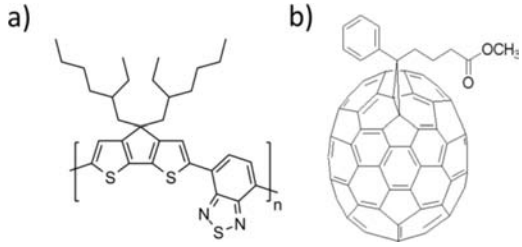

Received: November 7, 2011
Published: January 25, 2012

   dx.doi.org/10.1021/ja2104747 | *J. Am. Chem.Soc.* 2012, 134, 2884−2887

is known regarding the dynamics of the process. This understanding is lacking in part because of the relative ease with which new materials can be synthesized and screened in devices[17] and the difficulty of adequate morphological characterization of BHJ blends.[18−21] Herein, grazing-incidence wide-angle X-ray scattering (GIWAXS) has been used to observe the structural evolution of PCPDTBT:$PC_{70}BM$ active-layer films processed from CB with and without ODT. GIWAXS is a synchrotron-based X-ray technique that has been used extensively to provide structural insight into the crystallinity of organic thin films and blends.[22] Our studies have revealed that processing with ODT affects the initial polymer organization present in the incipient film as well as the kinetics of morphological development, which includes structural reorganization throughout a period of more than 40 min after the solution-casting step.

To ensure faithful reproduction of the structures evolved in functional BHJ devices (i.e., glass/ITO/PEDOT:PSS/PCPDTBT:$PC_{70}BM$ [ITO = indium tin oxide, PEDOT:PSS = poly(3,4-ethylenedioxythiophene):poly(styrene sulfonate)], the samples used for GIWAXS measurements were spin-cast from CB or CB containing 2−3% ODT atop PEDOT:PSS-coated Si wafers. The use of Si decreased the background X-ray scattering from ITO.[23] Identical PCPDTBT:$PC_{70}BM$ ratios (1:3), concentrations (10 mg/mL:30 mg/mL), and deposition conditions via spin-casting (1200 rpm for 60 s from a 60 °C solution, resulting in a film thickness of 80 nm) were used to replicate those previously reported for device optimization.[9] After spin-coating, the films were transferred onto a sample goniometer and oriented such that X-rays (λ = 0.0975 nm) were incident on the film at a grazing angle of 0.12°. After sample alignment (total time ∼2 min from spin-coating), a series of 2 min exposures were taken at 4 min intervals over a period of 78 min.

Figure 1 shows 3D GIWAXS sector plots from PCPDTBT:$PC_{70}BM$ films cast from CB containing 3% ODT after (a) 2, (b) 26, and (c) 78 min. These sector plots display the scattered intensity versus the scattering vector q and the polar angle χ (χ = 0° corresponds to the out-of-plane direction, i.e., parallel to the film normal). A procedure for generating sector plots from raw GIWAXS patterns is provided in the Supporting Information (SI). In contrast to the GIWAXS results from films processed from neat CB, which showed an amorphous, isotropic scattering pattern that remained unchanged from 2 to 78 min (see Figure 1d for the situation after 78 min and Figure S2 in the SI for the plot after 2 min), ODT-processed blends showed polymer crystallite formation within only 2 min after casting (Figure 1a). The presence of polymeric crystallites was signaled by three distinct scattering peaks: a set of two peaks [labeled (100) and (100)′, observed near 5 nm^{-1} and 5.5 nm^{-1}, respectively], which are attributed to two polymorphs with different periodic alkyl stacking arrangements,[13] and a third peak near 16.3 nm^{-1} [labeled (010)] assigned to face-to-face (π−π) stacking of the PCPDTBT backbone. The broad scattering feature arising near 14 nm^{-1} is attributed to scattering from the amorphous fraction of the film, with contributions from the amorphous $PC_{70}BM$ as well as from disordered PCPDTBT and possibly residual solvent or additive. Although the position of the amorphous scattering peak loosely indicates the presence of some characteristic packing distance, the large breadth of the peak indicates that ordering occurs over only very short ranges.[24]

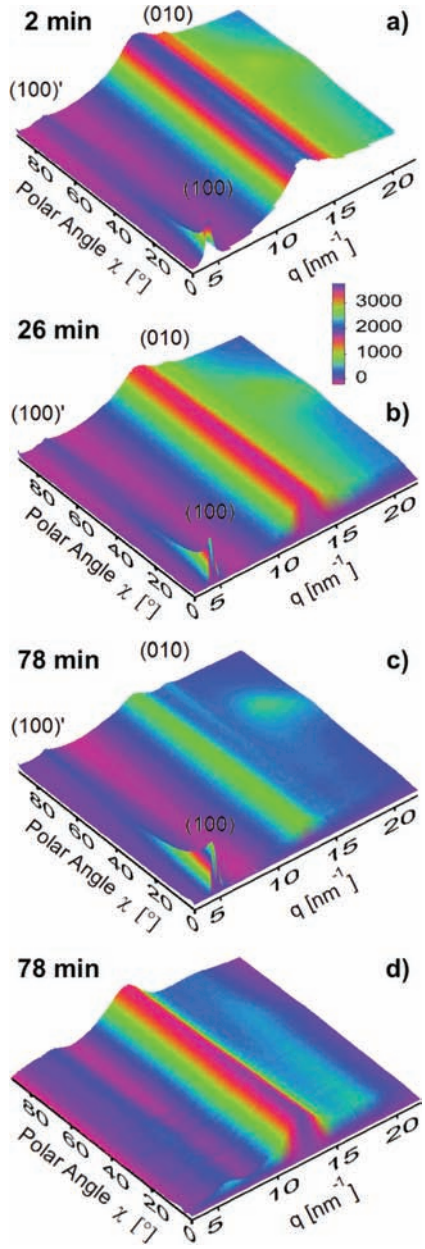

Figure 1. 3D sector plots of PCPDTBT:$PC_{70}BM$ blends cast from CB containing (a−c) 3% or (d) 0% ODT, showing the scattered intensity (linear color scale) vs polar angle χ and scattering vector q at times of (a) 2, (b) 26, and (c, d) 78 min after spin-coating.

The total scattered intensity from each specific crystallographic feature can be used to obtain information regarding the dynamics of film formation. The total scattered intensity was determined by separately fitting the individual line scan $I(\chi, q)$ at each polar angle χ. Specifically, the 1D scattering intensity curves [$I(q)$ at fixed χ] were fitted using a linear combination of Gaussian curves representing the contributions from (100), (100)′, (010), and amorphous scattering (see the SI). The results of this fitting procedure are provided in Figure 2, which shows how the positions of the (100) and (100)′ peaks changed between 2 and 78 min.

Further insight from the GIWAXS patterns can be obtained using a quantitative description of the orientation distribution of the crystallographic features in terms of an orientational

dx.doi.org/10.1021/ja2104747 | J. Am. Chem.Soc. 2012, 134, 2884−2887

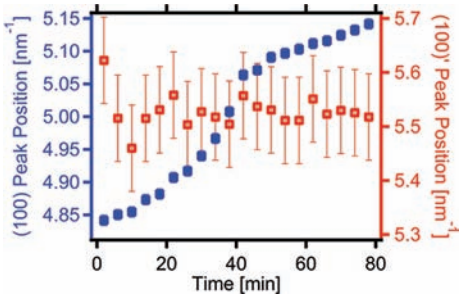

Figure 2. Positions of the (100) peak (blue) and the (100)′ peak (red) as functions of time, demonstrating the densification of (100) crystallites in a PCPDTBT:$PC_{70}BM$ film processed from CB containing 3% ODT.

order parameter S, given by[24]

$$S = \frac{1}{2}(3f_{\perp} - 1)$$

where the molecular orientation parameter $f_{\perp}$ used to represent the orientation of the polymeric crystallites relative to the axis normal to the surface is determined from the geometrically corrected scattered intensity $f(\chi)$ (see the SI):

$$f_{\perp} = \int_0^{\pi/2} \cos^2 \chi f(\chi)\, d\chi$$

From a practical perspective, S is a quantity that varies between −0.5 and 1, where a value of 1 (−0.5) indicates a parallel (orthogonal) orientation of the normal of a crystallographic plane relative to the substrate normal. Conversely, a completely isotropic distribution of the crystallographic planes leads to an S value of 0. Our analysis showed that although the (100), (100)′, and (010) peaks were present after only 2 min (Figure 1a), these features displayed markedly different orientations: $S_{(100)} = 0.67$, $S_{(100)'} = 0.25$, and $S_{(010)} = 0.01$. Figure 3 summarizes the time evolution of $S_{(100)}$ and $S_{(100)'}$ during film drying.

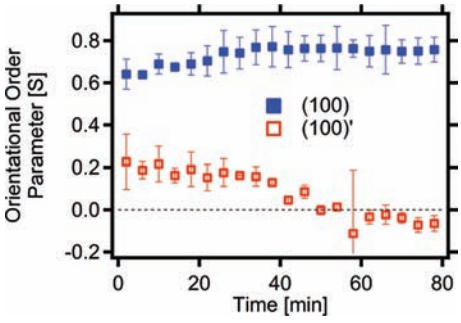

Figure 3. Time evolution of the orientational order parameters S calculated for the (100) and (100)′ crystallographic planes.

Differences in the scattering patterns can also be qualitatively observed by comparison of panels (a) and (b) of Figure 1. These changes indicate substantial structural modification over the first 26 min after casting. From Figure 2, one observes that the position of the alkyl chain stacking (100) peak shifted to higher q (from 4.85 to 4.9 nm^{-1}). From the relationship between q and the lattice spacing ($d = 2\pi/q$), we find a contraction of $d_{(100)}$ from 1.30 to 1.28 nm. As shown in Figure 3, $S_{(100)}$ increased slightly, from 0.67 to 0.75. The latter can be also noted in the plots in Figure 1a,b, which show a higher concentration of (100) scattered intensity near the out-of-plane direction. S shows the preference for crystallites to be arranged with their (100) planes either edge-on ($S = 1$) or plane-on ($S = -0.5$) relative to the substrate plane. The increase in $S_{(100)}$ with time suggests a physical picture in which early during the film drying process, polymeric crystallites rotate into a more edge-on orientation or new crystallites are preferentially nucleated with an edge-on orientation. Figure 3 also shows that during the first 26 min, in contrast to the (100) crystallites, the (100)′ peak evolved toward a less edge-on orientation [$S_{(100)'} = 0.18$]. Finally, it is worth noting that Figure 1a,b also indicates a decrease in the total scattered intensity from the amorphous regions of the film (also see Figure S4b).

Examination of Figure 1b,c shows that the morphological features continued to evolve after 26 min and that these changes were similar to those observed during the first 26 min of the film evolution. As shown in Figure 2, the (100) peak position was further shifted to higher q values (from 4.9 nm^{-1} at 26 min to 5.15 nm^{-1} at 78 min). The overall shift in q from 2 to 78 min corresponds to a 0.75 Å decrease in the (100) alkyl chain stacking distance. Figure 3 indicates that the population of the (100) crystallites exhibited a nearly constant edge-on character [$S_{(100)} = 0.76$] from 26 min onward. Conversely, the population of (100)′ crystallites appears to have rotated toward a plane-on orientation [$S_{(100)'} = -0.06$], although these are a distinct minority in the film. The time evolution of the features in Figure 1a−c is in striking contrast to the behavior observed from films processed from neat CB, which exhibited an amorphous, isotropic scattering pattern that remained unchanged over time (Figure 1d).

The composite set of data and analysis described thus far reveals that the ODT additive (i) induces ordering of PCPDTBT within a short period of time (less than 2 min) and (ii) enables structural reorganization of the film (particularly reorientation and densification of polymeric crystallites) throughout a remarkably long of period of time, at least in comparison with the conditions for films cast from CB alone. It is also important to note that none of the crystalline features observed in the ODT-treated BHJ blend could be attained by thermal annealing (Figure S2c).

The crystalline correlation length (CCL) can be estimated by the Scherrer equation:

$$\mathrm{CCL} = \frac{2\pi}{\mathrm{FWHM}}$$

where FWHM represents the full width at half-maximum of the Gaussian curve used to fit the scattering feature. This analysis shows that the CCL of the (100) peak was ∼9 nm over the course of the experiment (Figure S5).

Figure 4 compares the increase in the total scattered intensity from the (100) peak with the decrease in the total scattered intensity arising from the amorphous fraction of the film during the film drying process. The fact that increases in the total scattered intensity arising from the (100) crystallites were accompanied by no observable increase in their CCL values suggests that the crystalline fraction of the film increases as a result of additional nucleation processes rather than by further growth of existing crystallites. Similar population growth was not observed for the (100)′ crystallites, as the total scattered intensity from this feature did not change with time.

It is also interesting to note the similarities in the qualitative behavior of the position and the total scattered intensity of the (100) peak as functions of time. The changes in the peak

dx.doi.org/10.1021/ja2104747 | J. Am. Chem.Soc. 2012, 134, 2884−2887

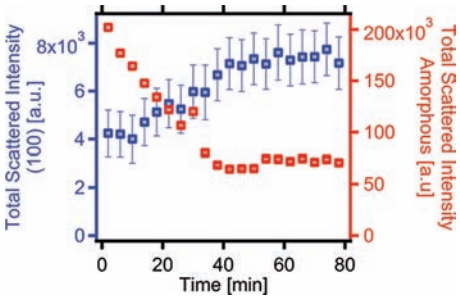

Figure 4. Total scattered intensities (i.e., integrated over all χ) from the (100) peak (blue) and the amorphous region (red) as functions of time after casting.

position were correlated with the changes in the crystalline fraction of the film [i.e., the total scattered intensity of the (100) peak]. In addition, the contribution to the amorphous scattered intensity attributed in part to scattering from ODT molecules was observed to decrease during this time. This result suggests that a small fraction of ODT is initially intermingled with the alkyl chains of the polymer and that the additional crystal nucleation occurs as the additive concentration decreases during drying. The larger fractional decrease of the amorphous scattering, relative to the smaller increase from the (100) scattering (Figure 4), is consistent with the notion that a larger fraction of residual ODT molecules are entrapped in the amorphous portions of the film.

Results from the temporally resolved in-situ GIWAXS experiments described here indicate that adding ODT to the CB solution from which PCPDTBT:$PC_{70}BM$ is cast simultaneously reduces the nucleation barrier for polymer crystallization during the initial film formation, facilitates crystallite reorientation, and allows for nucleation to occur during a prolonged film drying process. It is worth recalling that ODT has a much higher boiling point than CB (a feature common to the majority of solvent additives that improve BHJ organization), and thus, the gradual evaporation of ODT from the film may naturally explain the time dependence of the structural evolution. Notably, the PCPDTBT crystalline features could not be obtained by thermal annealing of the films. The results described herein provide concrete evidence that formation of the final organization of the conjugated polymer donor in BHJ blends takes a longer time than originally anticipated and that additives influence the processability by providing an environment in which polymer chains are sufficiently mobile for continued equilibration and reorganization.

■ ASSOCIATED CONTENT

Ⓢ Supporting Information

More detailed technical description of the generation of 3D sector plots from raw GIWAXS data; GIWAXS of non-additive-processed PCPDTBT:$PC_{70}BM$ films; GIWAXS line-scan fitting procedure; and calculation of S and CCL values. This material is available free of charge via the Internet at http://pubs.acs.org.

■ AUTHOR INFORMATION

Corresponding Author

bazan@chem.ucsb.edu; edkramer@mrl.ucsb.edu

■ ACKNOWLEDGMENTS

The authors are grateful to the Office of Naval Research (N000141110284) for support of the work. J.T.R. thanks the NSF for a Graduate Research Fellowship, the NSF ConvEne IGERT Program (NSF-DGE 0801627), and the Advanced Light Source for a doctoral fellowship. Portions of this research were carried out at the Stanford Synchrotron Radiation Lightsource (SSRL), a National User Facility operated by Stanford University on behalf of the U.S. Department of Energy, Office of Basic Energy Sciences.

■ REFERENCES

(1) Gunes, S.; Neugebauer, H.; Sariciftci, N. S. *Chem. Rev.* **2007**, *107*, 1324.
(2) Thompson, B. C.; Fréchet, J. M. J. *Angew. Chem., Int. Ed.* **2008**, *47*, 58.
(3) Blouin, N.; Michaud, A.; Gendron, D.; Wakim, S.; Blair, E.; Neagu-Plesu, R.; Belletete, M.; Durocher, G.; Tao, Y.; Leclerc, M. *J. Am. Chem. Soc.* **2008**, *130*, 732.
(4) Yu, G.; Gao, J.; Hummelen, J. C.; Wudl, F.; Heeger, A. J. *Science* **1995**, *270*, 1789.
(5) Erb, T.; Zhokhavets, U.; Gobsch, G.; Raleva, S.; Stuhn, B.; Schilinsky, P.; Waldauf, C.; Brabec, C. J. *Adv. Funct. Mater.* **2005**, *15*, 1193.
(6) Chan, S.-H.; Hsiao, Y.-S.; Hung, L.-I.; Hwang, G.-W.; Chen, H.-L.; Ting, C.; Chen, C.-P. *Macromolecules* **2010**, *43*, 3399.
(7) Morana, M.; Azimi, H.; Dennler, G.; Egelhaaf, H. J.; Scharber, M.; Forberich, K.; Hauch, J.; Gaudiana, R.; Waller, D.; Zhu, Z. H.; Hingerl, K.; van Bavel, S. S.; Loos, J.; Brabec, C. J. *Adv. Funct. Mater.* **2010**, *20*, 1180.
(8) Woo, C. H.; Beaujuge, P. M.; Holcombe, T. W.; Lee, O. P.; Fréchet, J. M. J. *J. Am. Chem. Soc.* **2010**, *132*, 15547.
(9) Peet, J.; Kim, J. Y.; Coates, N. E.; Ma, W. L.; Moses, D.; Heeger, A. J.; Bazan, G. C. *Nat. Mater.* **2007**, *6*, 497.
(10) Moon, J. S.; Takacs, C. J.; Cho, S.; Coffin, R. C.; Kim, H.; Bazan, G. C.; Heeger, A. J. *Nano Lett.* **2010**, *10*, 4005.
(11) Hoven, C. V.; Dang, X. D.; Coffin, R. C.; Peet, J.; Nguyen, T. Q.; Bazan, G. C. *Adv. Mater.* **2010**, *22*, E63.
(12) Lee, J. K.; Ma, W. L.; Brabec, C. J.; Yuen, J.; Moon, J. S.; Kim, J. Y.; Lee, K.; Bazan, G. C.; Heeger, A. J. *J. Am. Chem. Soc.* **2008**, *130*, 3619.
(13) Rogers, J. T.; Schmidt, K.; Toney, M. F.; Kramer, E. J.; Bazan, G. C. *Adv. Mater.* **2011**, *23*, 2284.
(14) Chen, H. Y.; Hou, J. H.; Zhang, S. Q.; Liang, Y. Y.; Yang, G. W.; Yang, Y.; Yu, L. P.; Wu, Y.; Li, G. *Nat. Photonics* **2009**, *3*, 649.
(15) Qin, R. P.; Li, W. W.; Li, C. H.; Du, C.; Veit, C.; Schleiermacher, H. F.; Andersson, M.; Bo, Z. S.; Liu, Z. P.; Inganas, O.; Wuerfel, U.; Zhang, F. L. *J. Am. Chem. Soc.* **2009**, *131*, 14612.
(16) Liang, Y. Y.; Xu, Z.; Xia, J. B.; Tsai, S. T.; Wu, Y.; Li, G.; Ray, C.; Yu, L. P. *Adv. Mater.* **2010**, *22*, E135.
(17) Cheng, Y.-J.; Yang, S.-H.; Hsu, C.-S. *Chem. Rev.* **2009**, *109*, 5868.
(18) Coffin, R. C.; Peet, J.; Rogers, J.; Bazan, G. C. *Nat. Chem.* **2009**, *1*, 657.
(19) Yang, X. N.; Loos, J.; Veenstra, S. C.; Verhees, W. J. H.; Wienk, M. M.; Kroon, J. M.; Michels, M. A. J.; Janssen, R. A. J. *Nano Lett.* **2005**, *5*, 579.
(20) Brabec, C. J.; Heeney, M.; McCulloch, I.; Nelson, J. *Chem. Soc. Rev.* **2011**, *40*, 1185.
(21) Giridharagopal, R.; Ginger, D. S. *J. Phys. Chem. Lett.* **2010**, *1*, 1160.
(22) DeLongchamp, D. M.; Kline, R. J.; Fischer, D. A.; Richter, L. J.; Toney, M. F. *Adv. Mater.* **2011**, *23*, 319.
(23) Tong, M.; Cho, S.; Rogers, J. T.; Schmidt, K.; Hsu, B. B. Y.; Moses, D.; Coffin, R. C.; Kramer, E. J.; Bazan, G. C.; Heeger, A. J. *Adv. Funct. Mater.* **2010**, *20*, 3959.
(24) Roe, R. J. *Methods of X-ray and Neutron Scattering in Polymer Science*; Oxford University Press: New York, 2000.